RaDICAL: A Monostatic Passive Radar Framework for Geometry-Aware Detection and Image Recognition

Vladimir Volman *

Posted Date: 25 March 2026

doi: 10.20944/preprints202603.1990.v1

Keywords: passive radar; monostatic passive radar; SUCA; deterministic frequency dither; dictionary-based recognition; waveform-domain recognition; QR-domain processing; reference-channel-free passive sensing

 doi:10.20944/preprints202603.1990.v1

Article

RaDICAL: A Monostatic Passive Radar Framework for Geometry-Aware Detection and Image Recognition

Vladimir Volman

Advanced High Frequency Branch (LCF), NASA, Glenn Recearch Center, Cleveland, USA;
vvolman02@gmail.com

Abstract

This paper presents the RaDICAL sensing framework, a monostatic passive radar concept that combines a Sparse Uniform Circular Array (SUCA), deterministic multi-frequency dither, and dictionary-based waveform recognition for target detection and classification. Rather than forming conventional spatial images or relying primarily on Doppler processing, RaDICAL encodes target geometry directly into a composite receiver waveform and performs hypothesis testing by matching measured signals to a library of predicted responses. The paper develops the SUCA-based signal model for point and extended targets and formulates recognition as a waveform-domain dictio-nary matching problem using normalized complex correlation and QR-domain process-ing. A reproducible MATLAB-based study evaluates waveform separability, probability of detection versus dictionary SNR, physical power balance, receiver operating char-acteristic (ROC) behavior, and detection performance versus illuminator EIRP. The results show that deterministic frequency dither produces distinctive composite wave-forms with strong hypothesis separability. ROC simulations demonstrate reliable detec-tion at physical SNR levels below those typical of classical single-pulse matched-filter detection, while EIRP-based analysis indicates feasible detection for targets ranging from large aircraft to small drones and pedestrians. These results support the feasibil-ity of waveform-domain passive sensing using deterministic spatial–frequency encoding and dictionary-based recognition.

Keywords: passive radar; monostatic passive radar; SUCA; deterministic frequency dither; dictionary-based recognition; waveform-domain recognition; QR-domain processing; reference-channel-free passive sensing

1. Introduction

Passive radar has long attracted interest because of its low probability of intercept, spectrum efficiency, and ability to exploit existing transmissions as illuminators of opportunity [2,3]. Classical passive radar architectures typically rely on a reference channel that provides a clean copy of the transmitted waveform, enabling matched filtering, bistatic range estimation, and Doppler processing. In practice, however, such reference channels are often difficult or impossible to obtain when illuminators are noncooperative, dynamically scheduled, weak at the receiver location, or strongly distorted by propagation and multipath effects. In addition, many passive radar techniques depend heavily on favorable waveform properties, long coherent integration times, or Doppler separation, which can become fragile in cluttered environments or for slow-moving and stationary targets [4].

These limitations motivate alternative passive sensing architectures in which the receiver itself provides the dominant source of structure used for detection and recognition. In prior work [1], the RaDICAL (Ranging, Detection, Imaging, Communications, Approach and Landing) framework introduced a reference-free passive sensing concept in which tar-get information is extracted directly from the received echo waveform through a controlled receiver architecture and hypothesis-driven

 doi:10.20944/preprints202603.1990.v1

processing. A conceptual overview of the RaDI-CAL framework is shown in Figure 1. Rather than reconstructing a conventional radar image or relying primarily on Doppler processing, RaDICAL forms a structured composite wave-form whose shape depends on target geometry and is then matched against a dictionary of predicted responses.

The key hardware element of the RaDICAL system is the Sparse Uniform Circular Array (SUCA), illustrated in Figure 2. Signals received at the individual SUCA elements are inde-pendently digitized and processed according to the receiver architecture shown in Figure 3. A deterministic multifrequency dither is applied across the receiver channels so that the spatial information contained in the received wavefront is transformed into a composite waveform with distinctive temporal and phase structure. As a result, target geometry is not inferred indirectly through image formation alone but is encoded directly into the received signal.

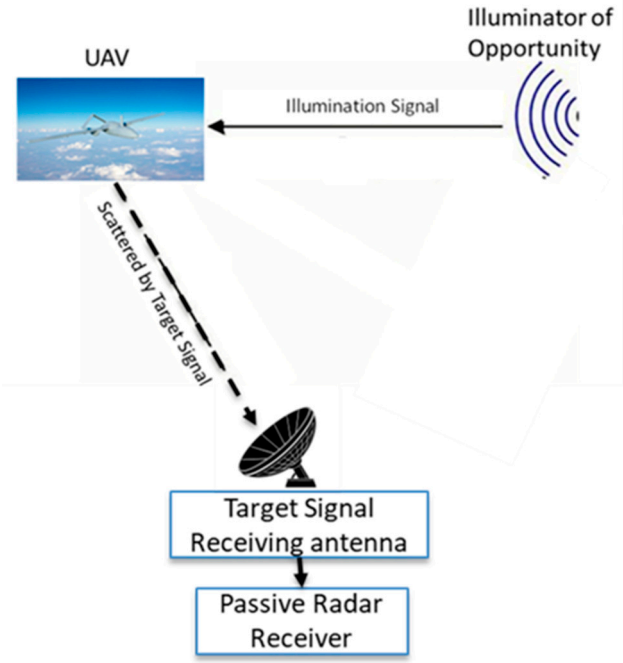

Figure 1. Conceptual overview of the RaDICAL monostatic passive radar architecture.

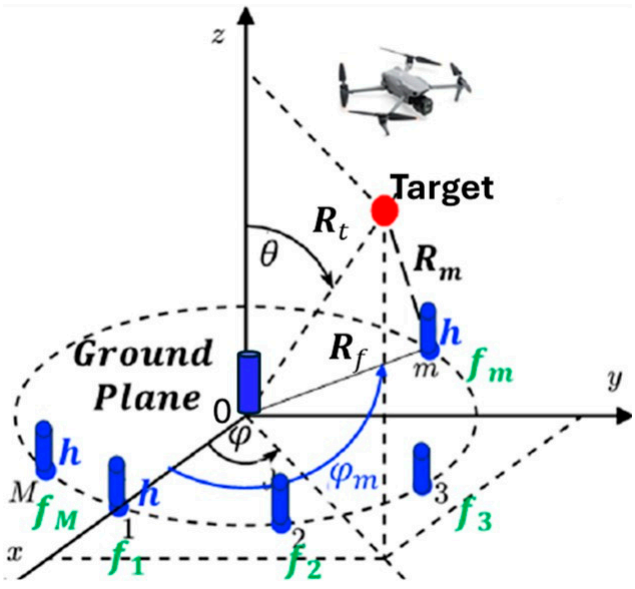

Figure 2. SUCA geometry with multifrequency dither.

 doi:10.20944/preprints202603.1990.v1

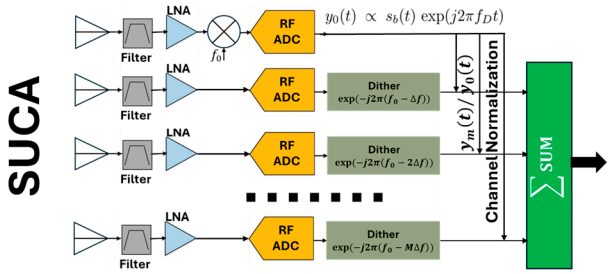

Figure 3. RaDICAL receiver architecture showing SUCA element channels, deterministic frequency dither, element0 normalization $z_m(t) = y_m(t)/y_0(t)$, and formation of the compos-ite waveform $E(t) = \sum_m z_m(t)$.

Within this framework, detection and recognition are formulated as a dictionary-matching problem. Offline-generated SUCA waveforms represent hypothesized target states or object classes, and the measured signal is compared with these reference responses using normal-ized complex correlation and QR-domain processing. This formulation naturally supports point-target detection, extended-target sensing, and image-based object recognition within a unified signal model. It also provides a direct way to evaluate system performance through waveform separability, physical signal-to-noise ratio, receiver operating characteristics, and illuminator power requirements.

The present paper develops and validates this concept using a reproducible MATLAB-based study. First, a SUCA signal model is introduced for point and extended targets under deterministic frequency diversity. Next, binary target images are converted into waveform-domain dictionary entries, allowing object recognition to be performed directly in the receiver waveform space. The study then examines the separability of these waveform dictionaries and validates the resulting sensing performance through several complementary metrics, in-cluding probability of detection versus dictionary SNR, power-balance feasibility, physical SNR performance, receiver operating characteristic (ROC) behavior, and detection proba-bility versus illuminator EIRP.

A central result of this paper is that performance in the RaDICAL framework is governed primarily by waveform structure rather than by nominal SNR alone. The broader perfor-mance metrics indicate that deterministic frequency dither and waveform-domain hypothesis matching enable robust detection at low physical SNR and under practical illumination conditions.

The remainder of this paper is organized as follows. Section II reviews related work in passive radar and reference-free sensing. Section III introduces the RaDICAL signal model for point and extended targets using the SUCA architecture with deterministic frequency diversity. Section IV formulates image recognition as a waveform-domain dictionary match-ing problem. Section V examines waveform dictionary separability. Section VI validates the RaDICAL framework using multiple performance metrics, including detection proba-bility versus dictionary SNR, power-balance analysis, detection probability versus physical SNR, ROC performance, and detection probability versus illuminator EIRP. Conclusions and future directions are given in Section VII.

2. Related Work and Literature Survey

More recent studies have explored detection and imaging using passive radar systems under a wider range of conditions. Aircraft detection and tracking using FM-radio-based passive radar has been demonstrated in operationally relevant scenarios [4], while broader tutorial treatments have traced the evolution of passive radar from detection to imaging applica-tions [12]. Passive synthetic aperture techniques have also been developed to enable image formation and velocity estimation for moving targets using illuminators of opportunity [9,10], although such methods typically rely on target motion and extended coherent integration intervals.

Several works have investigated passive radar imaging and target recognition using non-cooperative transmitters. Lanterman [11] presented early concepts for passive radar imaging and recognition, highlighting the challenges of reference signal availability and waveform uncertainty.

 doi:10.20944/preprints202603.1990.v1

More recent algorithmic advances have focused on efficient signal processing techniques for passive radar, including improved numerical conditioning and computational efficiency [8]. Comprehensive surveys have further emphasized the growing importance of passive sensing for UAV detection and monitoring, particularly in congested spectral envi-ronments [7].

A distinct line of research has examined *reference-free* passive sensing architectures. Bren-nan *et al.* [5] demonstrated reference-free passive RF imaging in the near field using dense spatial sampling and aperture-based processing, eliminating the need for a direct-path ref-erence signal in short- range imaging scenarios. Related work has explored reference-free WiFi radar approaches for monitoring people and drones [6], relying on spatial diversity and environmental scattering characteristics rather than explicit reference channels. While these methods successfully remove the reference antenna requirement, they generally depend on dense apertures, near-field assumptions, or spatial focusing for image formation.

Collectively, these works demonstrate a broad progression of passive radar capabilities, spanning detection, imaging, and recognition using noncooperative illuminators. The liter-ature reflects multiple complementary approaches, including Doppler-based detection, pas-sive synthetic aperture imaging, spatial aperture processing, and reference-free sensing in the near field. At the same time, existing methods typically emphasize one or more specific mechanisms—such as target motion, dense spatial sampling, near-field aperture processing, or detailed knowledge of the illuminating signal—which can constrain applicability across operating regimes. This diversity of approaches highlights the ongoing need for alterna-tive passive sensing frameworks that exploit receiver-side structure and hypothesis-driven processing to support robust operation under a wider range of conditions. Unlike these approaches, the RaDICAL framework uses a sparse receiver array together with determin-istic frequency diversity to encode target geometry directly into a composite waveform for dictionary-based recognition.

3. RaDICAL Signal Model

The SUCA shown in Figure 2 is a circular array consisting of a small number of elements: 11 elements placed on a ring of radius R_f and one central element with index 0, referred to as Element0, for a total of 12 receiving elements. All elements are low-gain receiving antennas, such as vertical monopoles or patch antennas above a ground plane. The spacing between adjacent ring elements is intentionally chosen close to one wavelength. This reduces mutual coupling and allows the array elements to operate nearly independently. Under this configuration, the signal received by the mth SUCA element can be written as

$$y_m(t; R_t, \theta_t, \phi_t) = \frac{C(t)}{R_m} \exp(j(2\pi f_0 t - k_0 R_m)), \quad (1)$$

where $R_0 = R_t$, $k_0 = 2\pi f_0/c$ is the wavenumber corresponding to the carrier frequency f_0, and c is the speed of light. The factor $C(t)$ denotes the common complex envelope of the received illumination and includes all multiplicative terms shared by the SUCA channels, such as the common element gain, transmitter modulation, illuminator–target propagation factor, target scattering coefficient, Doppler shift, and transmitter phase instabilities.

For a point target located at slant range R_t, azimuth ϕ_t, and elevation θ_t, the distance between the target and the mth element is

$$R_m(R_t, \theta_t, \phi_t) = \sqrt{R_t^2 + R_f^2 - 2R_t R_f \cos(\phi_t - \varphi_m)\cos\theta_t}, \quad (2)$$

where the angular position of each element is

$$\varphi_m = \frac{2\pi(m-1)}{M}, m = 1, \ldots, M \quad (3)$$

According to the receiver block diagram in Figure 3, the signal received by each SUCA element is digitized, while the Element0 signal is additionally downconverted to baseband,

 doi:10.20944/preprints202603.1990.v1

$$y_0(t; R_t, \theta_t, \phi_t) = \frac{C'(t)}{R_t} \exp(-jk_0 R_t). \quad (4)$$

Meanwhile, in the remaining channels ($m > 0$) a deterministic multifrequency dither shifts the carrier frequency according to the SUCA element index, $f_m = f_0 - m\Delta f$, where Δf is the frequency step (chosen as 1 MHz). The resulting signals can be written as

$$y_m(t; R_t, \theta_t, \phi_t) = \frac{C(t)}{R_m} \exp\big(j(2\pi f_m t - k_0 R_m)\big). \quad (5)$$

Here f_m denotes the digitally imposed dither frequency associated with the mth channel after digitization. Comparing (5) and (4), the received signals can be normalized with respect to y_0 to obtain

$$y_{norm,m}(t; R_t, \theta_t, \phi_t) = \frac{R_t}{R_m} \exp(-jk_0(R_m - R_t)) \exp(-j2\pi f_m t). \quad (6)$$

After normalization, all nuisance terms associated with the illumination signal—including the transmitter modulation $s(t)$, Doppler shift f_D, and phase instabilities $\phi(t)$ contained in the common factor $C(t)$—are automatically canceled. This property represents one of the key features of the RaDICAL architecture. In contrast to conventional passive radar systems, RaDICAL does not require knowledge of the transmitter signal structure. As a result, the full received waveform energy contributes to the spatial encoding process, enabling operation with a wide class of illuminators of opportunity without a dedicated reference channel.

Since the Element0 signal is downconverted to baseband purely digitally, this operation does not introduce additional mismatches relative to the remaining SUCA channels. Conse-quently, only conventional receiver-channel calibration (gain, phase, and delay alignment), similar to that routinely used in phased-array or MIMO radar systems, is required prior to normalization.

The composite RaDICAL receiver waveform is obtained by summing the contributions of all elements,

$$E(t; R_t, \theta_t, \phi_t) = \sum_{m=1}^{M} y_{norm,m}(t; R_t, \theta_t, \phi_t). \quad (7)$$

An extended object is modeled as a collection of L scattering centers with locations (R_ℓ, θ_ℓ, ϕ_ℓ) and complex reflectivities α_ℓ. Using (6), the composite waveform at the receiver output becomes

$$E(t; \mathcal{O}) = \sum_{\ell=1}^{L} \alpha_\ell \sum_{m=1}^{M} y_{norm,m}(t; R_\ell, \theta_\ell, \phi_\ell). \quad (8)$$

Thus, both the target location and its spatial structure are encoded in the composite wave-form $E(t; \mathcal{O})$, which serves as the fundamental observable of the RaDICAL sensing frame-work.

Figures 5 and 6 present the composite SUCA waveforms generated using the baseline formulation and the Element0-normalized formulation, respectively. In the complex plane, the waveforms corresponding to different targets follow distinct trajectories, illustrating the separability of the waveform dictionary. Element0 normalization suppresses common illumi-nation terms and keeps highlighting the differential spatial phase structure produced by the SUCA geometry.

Because the SUCA dwell time is 1 μs = $1/\Delta f$, variations associated with illumination modulation, Doppler, and phase instabilities remain nearly constant over this interval. Con-sequently, normalization primarily enhances the differential spatial phase structure that en-codes the target location and shape within the composite SUCA waveform.

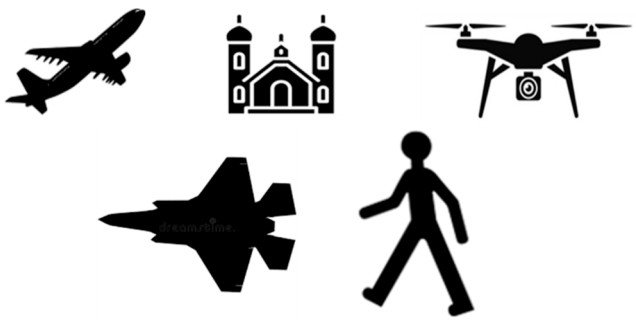

 doi:10.20944/preprints202603.1990.v1

Figure 4. Representative target images used to construct the object dictionary. From left to right: top row — Boeing 747, building, drone; bottom row — F–35 fighter jet, pedestrian.

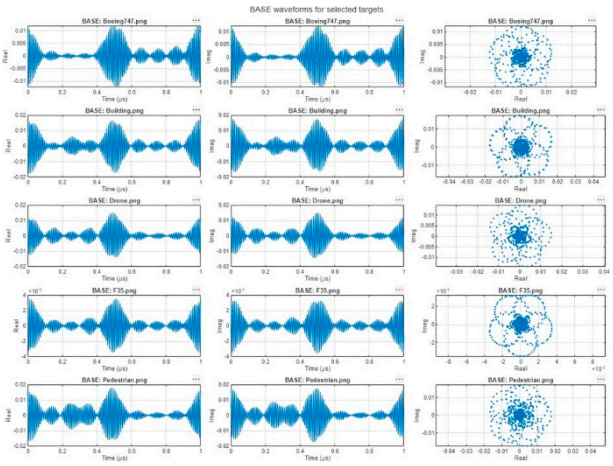

Figure 5. Composite SUCA waveforms for several representative targets generated using the baseline (BASE) formulation without element normalization. Each row corresponds to a different target from the image library.

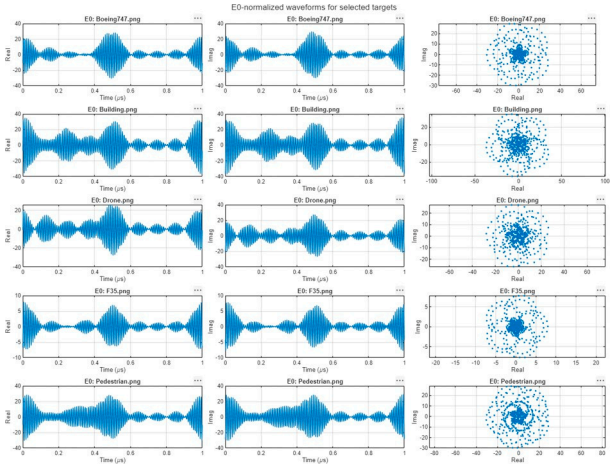

Figure 6. Composite SUCA waveforms for the same targets after element0 (E0) normaliza-tion.

4. Image Recognition via SUCA Waveform Dictionary

In the RaDICAL framework, target recognition is formulated as a waveform-domain dic-tionary matching problem. Rather than reconstructing a spatial image of the scene, the receiver directly compares the measured composite waveform with a set of precomputed reference waveforms corresponding to different object hypotheses.

Let $E(t)$ denote the composite waveform measured at the SUCA receiver. For each object hypothesis $\mathcal{O}_k$ in the dictionary, a reference waveform

$$E_k(t) \equiv E(t; \mathcal{O}_k) \quad (9)$$

is generated using the signal model described in the previous section. The collection of K reference waveforms forms the waveform dictionary

$$\mathcal{D} = \{E_1(t), E_2(t), \dots, E_K(t)\}. \quad (10)$$

Recognition is performed by evaluating a similarity metric between the measured waveform and each dictionary entry. In this work the similarity measure is the normalized complex correlation

$$\rho_k = \frac{|\langle E(t), E_k(t)\rangle|}{\|E(t)\|\|E_k(t)\|}, \quad (11)$$

where $\langle \cdot, \cdot \rangle$ denotes the complex inner product over the dwell interval. The object corre-sponding to the maximum correlation is selected as the recognition result.

 doi:10.20944/preprints202603.1990.v1

$$\hat{k} = \arg\max_{k} \rho_k \quad (12)$$

For numerical stability and efficient evaluation across large dictionaries, the waveform matrix

$$\mathbf{D} = \begin{bmatrix} E_1(t_1) & E_2(t_1) & \cdots & E_K(t_1) \\ \vdots & \vdots & \ddots & \vdots \\ E_1(t_N) & E_2(t_N) & \cdots & E_K(t_N) \end{bmatrix} \quad (13)$$

is orthogonalized using a QR decomposition

$$\mathbf{D} = \mathbf{QR}. \quad (14)$$

Matching is then performed in the QR domain, which preserves the correlation structure while improving numerical conditioning and reducing computational complexity when eval-uating large hypothesis sets.

Multiple dictionaries can be constructed offline for different operational scenarios, tar-get classes, or environmental conditions. During operation, the RaDICAL processor loads only the subset of dictionary entries required for the current sensing task. Consequently, scenario-specific dictionaries can be selected or updated dynamically, potentially under the guidance of higher-level control or AI-based decision logic. This approach enables scalable recognition capability while keeping the computational and memory requirements of the RaDICAL receiver modest. The short SUCA dwell time (1 μs in the present implementa-tion) enables rapid acquisition of independent waveform observations. This allows dictionary entries to be refined or adapted over time using newly collected data, enabling fast learning and environment-specific adaptation without modifying the receiver architecture.

An illustrative example of the recognition process is shown in Figure 14. The received waveform corresponds to a noisy measurement with SNR = −10 dB, where the time-domain signal itself does not visibly reveal the target structure. Conventional radar imaging sys-tems typically estimate the reflectivity of individual pixels from measured data, which often produces images that inherit measurement noise and reconstruction artifacts. In contrast, RaDICAL performs hypothesis recognition in waveform space. Once the correct hypothesis is identified, the corresponding target template from the dictionary can be displayed directly. Consequently, the displayed image shown in Figure 14 represents the recognized target model rather than a noise-contaminated pixel-by-pixel reconstruction of the received measurement. This approach preserves the structural features of the target and therefore supports more reliable target classification.

5. Waveform Dictionary Separability

Each target image in Figure 4 represents a distinct object hypothesis and is converted into a set of scattering centers according to the extended-object model in (8). For simplicity, the target images are converted to binary form: black pixels correspond to scattering centers with unit reflectivity α_ℓ = 1, while white pixels represent non-scattering regions with α_ℓ = 0. This uniform reflectivity assumption provides a baseline geometric representation of the target and can be replaced by measured reflectivity values when such data are available. In the simulations presented in this paper, targets are represented by their contours, where pixels located on the target boundary correspond to scattering centers. This representation em-phasizes the dominant geometric features of the object while keeping the number of effective scatterers small. Such contour-based representation is also consistent with the well-known electromagnetic scattering behavior of metallic objects, where strong radar returns are often associated with structural edges and surface discontinuities that concentrate induced surface currents.

Image-domain dictionary correlation is illustrated in Figure 7. Each bar represents the correlation coefficient (MATLAB *corrcoef*) between a reference image and all other dictionary entries in the absence of noise. The Boeing 747 image is selected as the reference and is indicated by the red marker. Low cross-correlation values confirm that the selected silhouettes are intrinsically distinct in the image domain.

 doi:10.20944/preprints202603.1990.v1

SUCA waveform separability. After SUCA encoding, each object hypothesis produces a distinct composite waveform $E_k(t)$ according to (8). Separability of the waveform dictionary is evaluated using the normalized complex correlation

$$\rho_{ij} = \frac{|\langle E_i, E_j \rangle|}{\|E_i\| \|E_j\|}, \quad (15)$$

where $\langle \cdot, \cdot \rangle$ denotes the complex inner product over the dwell interval. Low cross-correlation values indicate that the encoded SUCA waveforms corresponding to different targets remain well separated in the waveform domain.

Waveform-domain correlation between SUCA dictionary entries is shown in Figure 8. Each bar represents the normalized complex correlation between the reference waveform (Boe-ing 747) and all other dictionary waveforms. Although the composite waveforms exhibit higher correlation than the original images (Figure 7), the phase diversity introduced by the SUCA geometry preserves sufficient separability of the waveform dictionary. This analysis provides an empirical demonstration of waveform identifiability by evaluating the separabil-ity of dictionary waveforms generated by different target hypotheses.

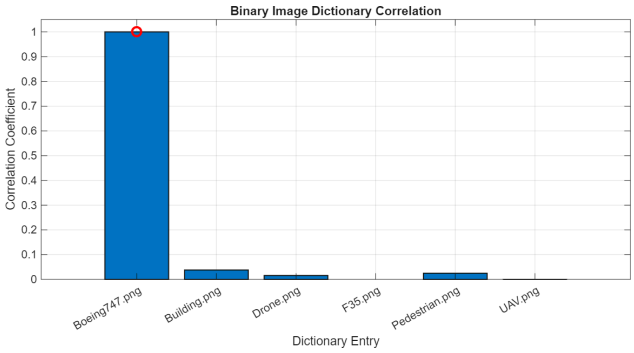

Figure 7. Image-domain correlation between binary dictionary images. Each bar represents the standard correlation coefficient (*corrcoef*) between a reference image and all other dic-tionary entries in the absence of noise. The Boeing 747 image is selected as the reference and is indicated by a red circle.

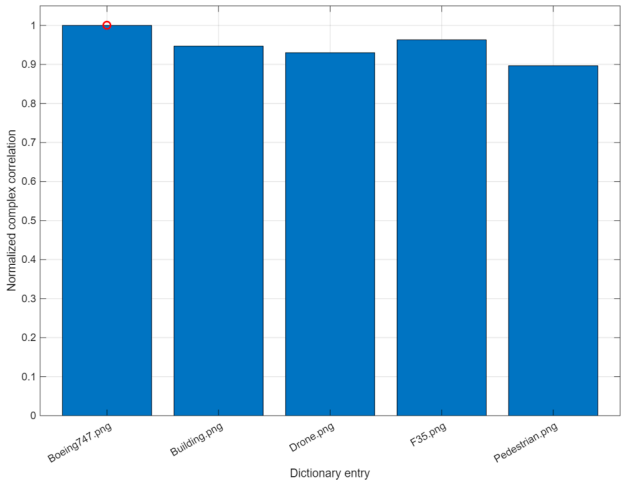

Figure 8. Waveform-domain correlation between SUCA dictionary entries for contour tar-gets. Each bar shows the normalized complex correlation between the Boeing 747 reference waveform and the remaining dictionary waveforms. The Boeing 747 image is selected as the reference and is indicated by a red circle.

6. RaDICAL Waveform Recognition Validation with Four Metrics

The waveform separability analysis of the previous section is now validated quantitatively using four complementary metrics. These metrics evaluate the recognition capability of the RaDICAL waveform dictionary, the physical signal power balance, and the resulting detec-tion performance

 doi:10.20944/preprints202603.1990.v1

under noise. Such validation follows the conventional radar performance evaluation framework described in classical detection analysis [13]. Specifically, the valida-tion includes:

(i) probability of detection P_d versus dictionary SNR defined with respect to the dictio-nary waveform power;
(ii) physical power-balance analysis and the corresponding physical signal-to-noise ratio SNR_{phys} derived from the signal and noise power obtained in the power-balance simulation;
(iii) probability of detection P_d versus SNR_{phys} under additive white Gaussian noise (AWGN);
(iv) receiver operating characteristic (ROC) performance.

Note that such performance metrics are standard in radar detection analysis and are applicable to both active and passive radar systems.

6.1. Detection Probability Versus Dictionary SNR

The first validation metric is illustrated in Figure 9, which shows the probability of cor-rect detection P_d as a function of the dictionary signal-to-noise ratio. As the dictionary SNR increases, the probability of correct detection rapidly approaches unity. The element-normalized (E_0) dictionary exhibits consistently higher detection probability in the low-SNR regime, indicating improved robustness of the normalized waveform representation. In par-ticular, reliable detection ($P_d \approx 1$) is achieved for SNR values above approximately −6 dB for both configurations.

The received signal is compared with all dictionary waveforms, and a detection is declared when the strongest correlation exceeds a fixed threshold. The results demonstrate strong radar detection performance even under severe noise conditions. In particular, significant detection probability is maintained at SNR levels below −15 dB, indicating that the RaDI-CAL waveform encoding and dictionary-based detection provide substantial discrimination capability without requiring long observation intervals or multi-dwell processing.

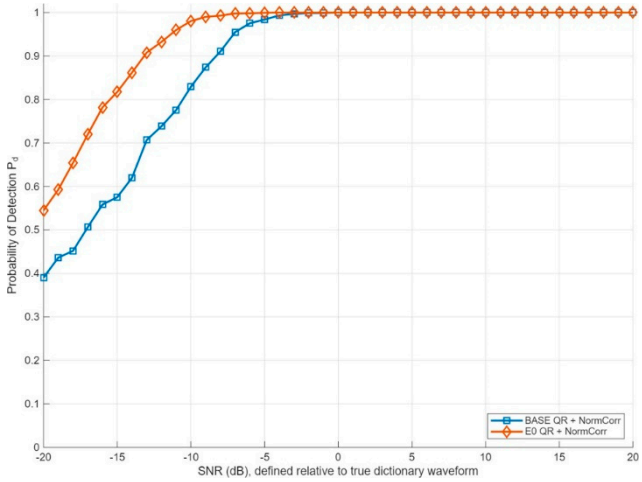

Figure 9. Probability of correct recognition P_d versus dictionary SNR for QR-based normal-ized correlation matching. Results are shown for the baseline (BASE) waveform and the element0-normalized ($E0$) dictionary.

6.2. Power-Balance Analysis

The second validation metric relates the composite waveform $E(t; O)$ in (8) to the minimum received signal power required for reliable detection. This detection threshold is computed from the receiver noise floor as

$$P_{req}[\text{dBm}] = -174 + 10\log_{10} \text{BW} + \text{NF} + \text{SNR}_{req} - \text{PG}, \quad (16)$$

where BW is the receiver bandwidth, NF is the receiver noise figure, SNR_{req} is the required detection SNR, and PG is the processing gain. It is assumed that the SUCA consists of $M = 11$ ring elements with ring radius $R_f = 4$ m, operating at $f_0 = 100$ MHz with a dither frequency step $\Delta f = 1$ MHz, which

 doi:10.20944/preprints202603.1990.v1

corresponds to a dwell time $T_{scan} = 1\ \mu s$. The illuminator–target range is $R_{it} = 20$ km, the target–receiver range is $R_{tr} = 2$ km, $SNR_{req} = 10$ dB, and BW = 1 MHz .

Figure 10 shows the received signal waveform power as a function of illuminator EIRP for representative target radar cross sections listed in the box. The horizontal dashed line indicates the minimum signal power required for reliable recognition, which is derived from the detection threshold of the QR-based correlation detector used in the previous subsec-tion. Intersection of the target curves with this threshold therefore indicates the minimum illuminator EIRP required for successful detection.

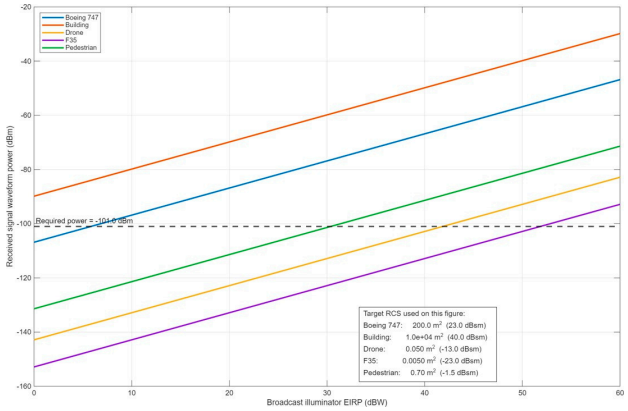

Figure 10. Received signal waveform power versus illuminator EIRP for representative target radar cross sections. The dashed line indicates the minimum received power required for detection.

Large targets such as aircraft or buildings exceed the required signal level even for mod-erate illuminator power levels. Smaller targets such as drones and pedestrians require higher illuminator EIRP but still reach the detection threshold within realistic ranges for modern communication satellites or broadcast transmitters. Even very small radar cross sections, such as the F-35 example, remain detectable when sufficient illumination power is available. This analysis confirms that the RaDICAL waveform-recognition framework is feasible under realistic illumination levels and that the required signal power is compatible with practical broadcast illuminators of opportunity. The numerical values shown in Figure 10 correspond to the assumed receiver parameters and representative target radar cross sections used in this analysis. In practice, the exact detection threshold and required illuminator EIRP may vary depending on receiver implementation, processing parameters, and the actual target orientation and radar cross section.

6.3. Detection Probability Versus Physical SNR

The third validation metric evaluates the probability of detection as a function of the physical signal-to-noise ratio at the receiver. The physical SNR is defined as the ratio between the received waveform power and the receiver noise power computed from (16). Figure 11 shows the resulting probability of detection P_d versus the physical SNR_{phys} obtained using the QR-based normalized correlation detector described in the previous sections. As expected, the probability of detection increases monotonically with increasing SNR. Stricter false-alarm requirements shift the detection curves toward higher SNR values. Nevertheless, reliable detection ($P_d \approx 1$) is achieved at physical SNR levels around −15 dB for all considered false-alarm probabilities, demonstrating strong detection capability of the RaDICAL waveform-recognition framework under realistic receiver noise conditions. For comparison, classical radar detection theory indicates that reliable single-pulse detection generally requires SNR values on the order of several decibels depending on the desired P_d and P_{fa} (see [13], pp. 252–255).

 doi:10.20944/preprints202603.1990.v1

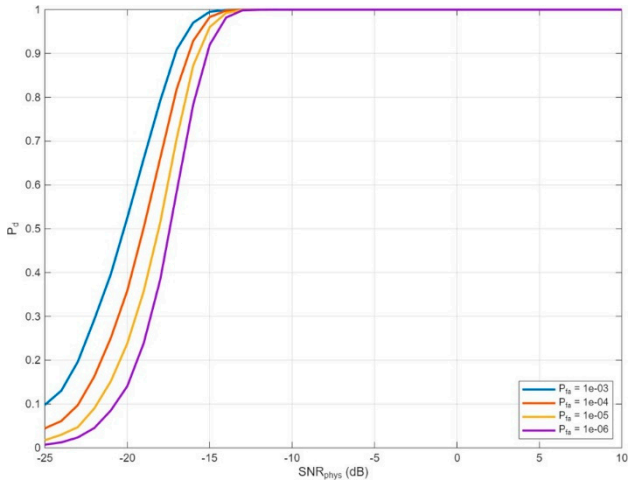

Figure 11. Detection probability P_d as a function of physical SNR for different false-alarm probabilities P_{fa}.

This result is consistent with the processing gain obtained from the deterministic wave-form structure exploited by the dictionary detector.

6.4. Receiver Operating Characteristic (ROC)

The final validation metric is the receiver operating characteristic (ROC) curve, which pro-vides a standard performance measure for binary detection problems by plotting the prob-ability of detection P_d versus the probability of false alarm P_{fa} as the detection threshold varies. Figure 12 shows a family of ROC curves corresponding to different physical signal-to-noise ratio levels for the Boeing 747 target waveform used in the simulation. As expected, increasing SNR shifts the ROC curves toward the upper-left corner of the diagram, indicating improved detection performance. Even at relatively low physical SNR values the detector maintains high detection probability for moderate false-alarm levels. For example, the ROC curve corresponding to SNR_{phys} = −18 dB shows that the probability of detection exceeds 0.9 at approximately $P_{fa} \approx 10^{-2}$. For SNR_{phys} = −15 dB the curve approaches the upper boundary of the diagram, indicating near-perfect detection across most of the false-alarm probability range considered.

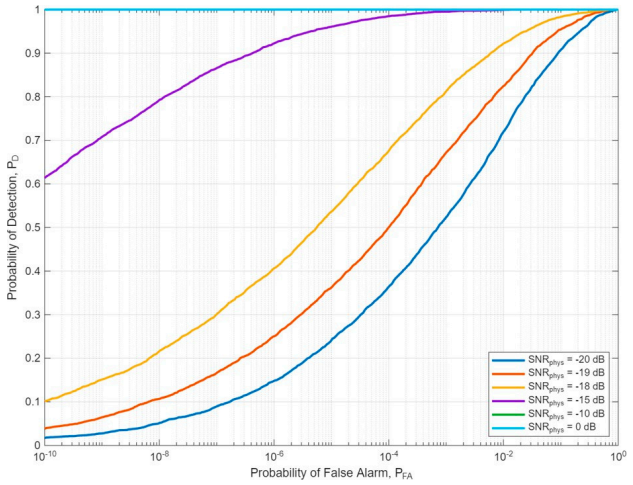

Figure 12. Receiver operating characteristic (ROC) curves showing the probability of detec-tion P_d versus false-alarm probability P_{fa} for several physical SNR levels.

For comparison, classical radar detection theory indicates that reliable single-pulse de-tection generally requires near-zero or positive SNR depending on the desired detection probability P_d and false-alarm probability P_{fa}. As illustrated by the matched-filter ROC curves in Fig. 6.2 of Richards [13],

 doi:10.20944/preprints202603.1990.v1

achieving $P_d \approx 0.9$ typically requires SNR values on the order of 9–13 dB for commonly used false-alarm levels.

In contrast, the ROC curves obtained for the RaDICAL framework indicate high detec-tion probabilities at substantially lower physical SNR levels. This behavior arises because the RaDICAL waveform contains deterministic structure across multiple frequencies and tempo-ral samples. The matched waveform test therefore performs coherent integration across these components. In addition, extended targets are modeled as collections of multiple scattering centers, producing a structured waveform that can be matched coherently with the corre-sponding dictionary hypothesis. The resulting integration provides substantial processing gain relative to the classical single-pulse matched-filter model.

Improved detection performance resulting from spatial or waveform diversity has been widely discussed in MIMO radar systems [14,15]. In such systems, multiple observations improve the statistical separation between the hypotheses H_0 and H_1, leading to steeper ROC curves and improved detection performance. The RaDICAL framework exhibits a similar effect, where the diversity arises from deterministic frequency dither, temporal sampling, and the extended-target structure encoded in the waveform dictionary.

6.5. Detection Performance Versus Illuminator EIRP

To evaluate the practical sensitivity of the RaDICAL framework, the probability of detec-tion shown in Figure 13 was computed as a function of the illuminator EIRP for several rep-resentative targets. The results illustrate the illumination levels required to achieve reliable detection for targets with different radar cross sections.

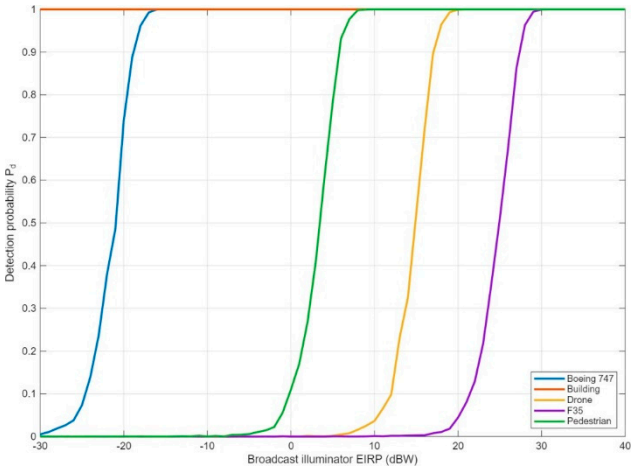

Figure 13. Detection probability P_d as a function of broadcast illuminator effective isotropic radiated power (EIRP) for several representative targets.

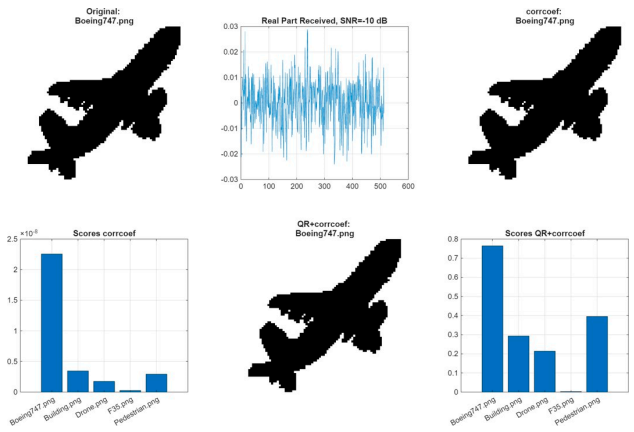

 doi:10.20944/preprints202603.1990.v1

Figure 14. Illustration of RaDICAL waveform recognition. Top left: binary template of the Boeing 747 target used in the dictionary. Top center: real part of the received composite waveform at SNR = −10 dB. Bottom left: correlation scores obtained using conventional corrcoef matching across several dictionary hypotheses. Bottom right: scores obtained using the proposed QR+normalized correlation detector, where the correct hypothesis (Boeing 747) produces the dominant response and the corresponding clean target template can be identi-fied from the dictionary despite the noisy received waveform.

For large radar cross-section objects such as commercial aircraft ($\sigma \approx 200$ m^2), reliable detection is achievable with relatively low illumination power. In the present geometry (target–receiver range $R_{tr} = 2$ km), the simulation indicates that detection of a Boeing 747-sized target becomes possible even for illuminator powers below 0 dBW.

For targets with smaller radar cross sections the required illumination power increases accordingly. For example, a low-RCS aircraft such as an F-35 ($\sigma \approx 0.005$ m^2) may require illumination levels on the order of 25–30 dBW. Moderate-size targets such as pedestrians ($\sigma \approx 0.7$ m^2) can still be detected at illumination levels of approximately 5–10 dBW, while small aerial vehicles such as drones ($\sigma \approx 0.05$ m^2) fall between these regimes.

These results indicate that, in addition to high-power broadcast transmitters, moderate-power local transmitters could potentially serve as illuminators for short-range sensing ap-plications such as traffic monitoring, navigation assistance, or airspace awareness.

For comparison, conventional passive bistatic radar systems typically perform detection by cross-correlating the received surveillance signal with a separately reconstructed reference signal from the illuminator of opportunity. In such systems, detection performance is primar-ily determined by the available signal-to-noise ratio, the coherent integration time, and the bistatic geometry of the transmitter, target, and receiver ([16], Chapters 5–6). Consequently, reliable detection often requires sufficiently stronger illumination and long observation inter-vals in order to accumulate adequate signal energy.

In contrast, the RaDICAL framework does not rely on reference-channel reconstruction or classical cross-correlation processing. Instead, deterministic frequency dither applied across the SUCA elements produces a structured waveform that encodes the spatial geometry of the target directly in the received signal. The recognition process therefore integrates determin-istic signal components across multiple frequencies and temporal samples. This structured integration increases the statistical separation between the hypotheses H_0 and H_1 and allows reliable detection at lower physical SNR levels and shorter observation dwell times.

7. Conclusion

This work introduced the RaDICAL sensing framework, a passive radar architecture that combines a sparse uniform circular array (SUCA), deterministic frequency dither, and wave-form–domain dictionary recognition. In contrast to conventional passive bistatic radar sys-tems that rely primarily on cross-correlation processing and long coherent integration times, the RaDICAL framework exploits deterministic frequency diversity across the SUCA ele-ments to produce a composite receiver waveform whose structure depends on the target geometry.

The performance metrics presented in this work confirm the viability of this concept. Re-ceiver operating characteristic simulations demonstrate reliable detection at physical signal-to-noise ratios significantly below those typically associated with classical single-pulse matched-filter detection. Additional analysis of detection probability versus illuminator EIRP illus-trates the illumination levels required for different classes of targets. Large radar cross section objects such as commercial aircraft can be detected with very low illumination power, while smaller targets such as pedestrians, drones, and low-observable aircraft require progressively higher but still practical illumination levels.

An important property of the RaDICAL framework is the interpretation of the waveform dictionary as a hypothesis filter in waveform space. Only targets whose predicted waveforms are

 doi:10.20944/preprints202603.1990.v1

present in the dictionary produce strong correlation responses, while objects not repre-sented in the hypothesis set are naturally rejected. Because detection is based on normalized waveform correlation, the method is also relatively robust to amplitude variations caused by moderate multipath effects.

Future work will focus on experimental validation using a prototype RaDICAL receiver system and on extending the waveform dictionary to more detailed three-dimensional target models. The architecture also lends itself naturally to distributed sensing, where multiple receivers operating with common illuminators of opportunity could provide large-area passive surveillance and improved localization accuracy.

Overall, the results suggest that structured waveform encoding combined with physics-based dictionary recognition offers a promising direction for next-generation passive sensing systems and shifts the emphasis of radar sensing from transmit power and long coherent integration toward structured waveform information content.

References

1. V. Volman, "Nonlinear SUCA Waveforms and QR-Domain Maximum-Likelihood Detection for Passive RaDICAL Monostatic Radar," *TechRxiv*, 2025, doi:10.36227/techrxiv.176404163.34190144.
2. H. D. Griffiths, C. J. Baker, and S. Papatsoris, "Passive coherent location radar sys-tems," *IEE Proc. Radar, Sonar and Navigation*, vol. 152, no. 3, pp. 153–159, 2003.
3. P. E. Howland and D. Maksimiuk, *"FM radio based bistatic radar,"* IEE Proceedings Radar, sonar and navigation, Vol. 152, No. 3, pp. 107-115, 2005.
4. F. Colone, K. Woodbridge, and P. Maresca, "Aircraft detection using FM radio-based passive radar," *IEEE Transactions on Aerospace and Electronic Systems*, vol. 46, no. 2,
5. pp. 689–705, 2010.
6. P. Brennan, K. Chetty, W. Li, S. Vishwakarma, F. Colone, and A. Amiri, "Reference-Free Passive RF Imaging Using Near-Field Spatial Processing," in *Proc. 2024 Int. Conf. on Computing, Internet of Things and Microwave Systems (ICCIMS)*, July 2024, Gatineau, QC, Canada, doi: 10.1109/ICCIMS61672.2024.10690411.
7. M. Di Seglio, F. Filippini, C. Bongioanni, and F. Colone, "Comparing reference-free WiFi radar sensing approaches for monitoring people and drones," in *Proc. RADAR 2022 – International Conference on Radar Systems*, Edinburgh, UK, 2024, vol. 18, no. 1, pp. 107–124.
8. Z. Tang, H. Ma, Y. Qu, and X. Mao, "UAV Detection with Passive Radar: Algo-rithms, Applications, and Challenges," *Drones*, vol. 9, no. 1, p. 76, Jan. 2025, available: https://doi.org/10.3390/drones9010076
9. M. Meller, "Efficient Signal Processing Algorithms for Passive Radars," in *Proc. NATO STO Meeting Proceedings STO-MP-SET-187*, NATO Science and Technology Organization, pp. 12-1–12-14, available: https://publications.sto.nato.int/ publications/STO%20Meeting%20Proceedings/STO-MP-SET-187/MP-SET-187-12. pdf.
10. S. Wacks and B. Yazıcı, "Passive synthetic aperture hitchhiker imaging of ground mov-ing targets – Part 1: Image formation and velocity estimation," *IEEE Trans. Image Process.*, vol. 23, no. 6, pp. 2487–2500, 2014.
11. S. Wacks and B. Yazıcı, "Passive synthetic aperture hitchhiker imaging of ground mov-ing targets – Part 2: Performance analysis," *IEEE Trans. Image Process.*, vol. 23, no. 9,
12. pp. 4126–4138, 2014.
13. A. D. Lanterman, "Passive radar imaging and target recognition using illumi-nators of opportunity," in *Proc. RTO SET Symposium on Target Identification and Recognition Using RF Systems*, Oslo, Norway, Oct. 11–13, 2004 (RTO-MP-SET-080), available: https://publications.sto.nato.int/publications/STO% 20Meeting%20Proceedings/RTO-MP-SET-080/MP-SET-080-24.pdf.
14. K. Kulpa, M. Malanowski, and P. Samczyński, "Passive Radar: From Detection to Imaging," Tutorial presented at *IEEE Radar Conference (RadarConf'19)*, Boston, MA, USA, 2019.
15. M. A. Richards, *Fundamentals of Radar Signal Processing*, 2nd ed. (McGraw-Hill, New York, NY, USA, 2014).
16. J. Li and P. Stoica, "MIMO Radar with Colocated Antennas," *IEEE Signal Processing Magazine*, vol. 24, no. 5, pp. 106–114, 2007.

 doi:10.20944/preprints202603.1990.v1

17. A. M. Haimovich, R. S. Blum, and L. J. Cimini, "MIMO Radar with Widely Separated Antennas," *IEEE Signal Processing Magazine*, vol. 25, no. 1, pp. 116–129, 2008.
18. H. D. Griffiths and C. J. Baker, *An Introduction to Passive Radar* (Artech House, 2017).